The Journal of Experimental Biology 211, 196-205
Published by The Company of Biologists 2008
doi:10.1242/jeb.005629

Research article

Flow patterns of larval fish: undulatory swimming in the intermediate flow regime

Ulrike K. Müller*, Jos G. M. van den Boogaart and Johan L. van Leeuwen

Experimental Zoology Group, Wageningen Institute of Animal Sciences (WIAS), Wageningen University, Marijkeweg 40, 6709 PG Wageningen, The Netherlands

*Author for correspondence at present address: Department of Biology, California State University Fresno, 2555 E San Remon Avenue, Fresno, CA 93740, USA (e-mail: umuller@csufresno.edu)

Accepted 5 July 2007

Summary

Fish larvae, like many adult fish, swim by undulating their body. However, their body size and swimming speeds put them in the intermediate flow regime, where viscous and inertial forces both play an important role in the interaction between fish and water. To study the influence of the relatively high viscous forces compared with adult fish, we mapped the flow around swimming zebrafish (*Danio rerio*) larvae using two-dimensional digital particle image velocimetry (2D-DPIV) in the horizontal and transverse plane of the fish. Fish larvae initiate a swimming bout by bending their body into a C shape. During this initial tail-beat cycle, larvae shed two vortex pairs in the horizontal plane of their wake, one during the preparatory and one during the subsequent propulsive stroke. When they swim 'cyclically' (mean swimming speed does not change significantly between tail beats), fish larvae generate a wide drag wake along their head and anterior body. The flow along the posterior body is dominated by the undulating body movements that cause jet flows into the concave bends of the body wave. Patches of elevated vorticity form around the jets, and travel posteriorly along with the body wave, until they are ultimately shed at the tail near the moment of stroke reversal. Behind the larva, two vortex pairs are formed per tail-beat cycle (the tail beating once left-to-right and then right-to-left) in the horizontal plane of the larval wake. By combining transverse and horizontal cross sections of the wake, we inferred that the wake behind a cyclically swimming zebrafish larva contains two diverging rows of vortex rings to the left and right of the mean path of motion, resembling the wake of steadily swimming adult eels. When the fish larva slows down at the end of a swimming bout, it gradually reduces its tail-beat frequency and amplitude, while the separated boundary layer and drag wake of the anterior body extend posteriorly to envelope the entire larva. This drag wake is considerably wider than the larval body. The effects of the intermediate flow regime manifest as a thick boundary layer and in the quick dying-off of the larval wake within less than half a second.

Key words: undulatory swimming, burst and coast, C-start, wake structure, particle image velocimetry, DPIV, fish larvae, *Danio rerio*.

Introduction

Many organisms, ranging in size from sperm cells to whales, swim by undulating their body. Although undulatory swimmers can use very similar propulsive movements, they do not necessarily employ similar propulsion mechanisms. Propulsion, in particular the fluid-dynamic interaction between organism and water, can differ drastically if body size differs by orders of magnitude. As body size drops, so does absolute swimming speed. Small, slow swimmers experience mainly viscous forces while large, fast swimmers experience mainly inertial forces (Videler, 1993). The ratio of inertial to viscous forces is expressed by the Reynolds number *Re*, which can be computed from the swimming speed U, body length L of the fish, and kinematic viscosity of the water ν: $Re=UL/\nu$.

Fish, in particular Actinopterygii, swim at a uniquely large range of Reynolds numbers during their life history. Hatchling fish are usually a few millimetres long, employing swimming speeds in the range 10–60 $L\ s^{-1}$ (Fuiman, 2002; Müller and Van Leeuwen, 2004). The corresponding Reynolds numbers range from 10 to 900 and put hatchlings into an intermediate flow regime, in which both viscous and inertial flow forces play important roles (Fuiman and Batty, 1997; McHenry and Lauder, 2005). As they grow and become faster swimmers, fish larvae experience a gradual change in the flow regime as the balance slowly tips from viscous to inertial forces (McHenry and Lauder, 2005). As juveniles grow into adults, *Re* can increase up to 10^5, which corresponds to the inertial flow regime.

Flow regime constrains which mechanisms are available for undulatory swimming: the smallest undulatory swimmers need to rely on viscous forces (skin friction) to generate thrust (McHenry et al., 2003); in larger, faster swimmers, pressure forces (e.g. lift-based thrust and acceleration reaction) come into play (Webb and Weihs, 1986). Undulating movements can generate thrust in a range of flow regimes, by exploiting viscous or inertial mechanisms, yet use similar motion patterns and even similar locomotory geometries (Taylor, 1952; McHenry et al., 2003; Videler, 1993). Undulatory swimming therefore suits the demands of fish that pass through a range of flow regimes during their life history.

In recent years, much progress has been made in understanding how undulatory swimmers interact with water to propel themselves. Undulatory swimmers have been documented to shed at least two types of wake: carangiform swimmers shed connected vortex loops (Blickhan et al., 1992; Müller et al., 1997; Nauen and Lauder, 2002) and anguilliform swimmers shed individual vortex rings (Müller et al., 2001; Tytell and Lauder, 2004). The shape and arrangement of

these vortex rings depends on the shape and arrangement of the trailing edges which the vortices are shed off, in particular the position, height and shape of the tail and unpaired fins (Nauen and Lauder, 2002; Drucker and Lauder, 2005; Tytell, 2006), and the phase relationship between their oscillations (Gopalkrishnan et al., 1994). The shedding pattern further depends on swimming speed (Tytell, 2004a), the ratio of swimming speed to body wave speed (Müller et al., 2002), and the shape of the body wave (Liao et al., 2003). The wake reflects the momentum transfer from fish to water, and therefore responds to changes in the fish's momentum, such as accelerations, by changing the orientation of the vortex rings (Tytell, 2004b). However, most studies have focused on fish swimming cyclically in the inertial flow regime. Relatively few flow studies have mapped the flow during accelerations and turns (Müller et al., 2000; Tytell, 2004b; Wolfgang et al., 1999). The few flow studies around undulatory swimmers in the intermediate and viscous flow regime have so far focused on the wake rather than the relationship between the body movements and the resulting flow (e.g. Brackenbury, 2001; Brackenbury, 2002; Brackenbury, 2003; Brackenbury, 2004; Müller et al., 2000).

Here, we document the flow patterns generated by larval zebrafish, which swim in the intermediate flow regime. As a first step to understanding how fish larvae swim by undulating their body, we will relate time-resolved flow patterns along the body and in the wake to swimming kinematics. In the future, computational flow studies (in collaboration with H. Liu) will complement this experimental approach, in order to provide the force data that are necessary to understand propulsive mechanics. In the present study, we focus on the three phases of a spontaneous swimming bout: (1) starting (acceleration phase), (2) swimming steadily (constant mean speed) and (3) gradually ceasing active propulsion (deceleration phase). Apart from mapping flow patterns onto body movements, we also pay special attention to how the relatively high viscous forces affect the flow patterns around these small undulatory swimmers compared with swimmers in the inertial flow regime.

Materials and methods

Fish

Zebrafish (*Danio rerio* Hamilton 1822) larvae were reared in the laboratory from wild-type parents. Eggs and larvae were held in batches of ~50 individuals in 1 l jars filled with aerated water at 28°C. Eggshells and debris were removed manually to reduce fouling, and the water was replaced every 2–3 days. The rearing temperature was kept at a constant 28°C by half submerging the jars in a large tank filled with temperature-controlled water and placed in a temperature-controlled room. The eggs and larvae were maintained at a 12 h:12 h light:dark cycle. The larvae were fed *Paramecium* (5 days post-fertilisation; d.p.f.) twice a day. For our experiments, we used sibling larvae 2, 3, 4 and 5 d.p.f. From 2 to 5 d.p.f., larval body length L increased from 3.4±014 mm (N=10) to 4.4±0.10 mm (N=10), respectively.

Flow recordings

To record swimming behaviour, 5–10 sibling larvae were transferred to a small filming tank (inner dimensions 50×50 mm; water level 10 mm; water temperature 27°C) 2–4 h after the last feeding period and allowed to acclimate for 0.5 h. The water was seeded with small Nylon beads (Degussa Vestosint; diameter 6 μm; density 1016 kg m^{-3}; seeding density 0.04–0.05 pixel^{-1} or 5000–6000 particles mm^{-3}). Flow fields were recorded with a high-speed digital camera (Redlake MotionPro, San Diego, CA, USA; 500, 800 or 1000 frames s^{-1}, 1260×1024, 1260×680, or 1280×512 pixels, exposure time 250 μs) and a macro lens (Nikon Micro 105 mm 2.8, f stop 5.6, with a 27.5 mm extension ring) mounted above the aquarium. The long axis of the field of view was 8.3 mm. We used a 400 mm (focal length) plan-convex lens and 63 mm (focal length) plan-cylindrical lens to generate a light sheet from the beam of a continuous Argon ion laser (max. power 2 W, Coherent Innova 90). In the filming area, the light sheet was 25 mm wide and 0.2 mm thick.

Young zebrafish larvae tend to sink to the bottom of the tank and hence initiate almost all swimming bouts from or near the bottom of the tank. During cyclic swimming bouts, the larva maintains a constant mean swimming speed for several tail beats (average of instantaneous speed per tail beat) (Müller and van Leeuwen, 2004). The larvae first swim up and away from the bottom and then level their path near the top of the tank and start to swim cyclically. Also brief swimming bursts and turns are occasionally executed well clear of the bottom. During brief bursts, the larva accelerates and then decelerates, without maintaining a constant mean swimming speed for several tail beats (Müller and van Leeuwen, 2004). In order to record flow fields with the least bottom effects, the light sheet was situated 2–3 mm (4–6 maximum body heights) below the glass lid of the film tank. All recorded swimming behaviour was either spontaneous or a response to the presence of other larvae. We recorded 200 swimming sequences from 10 randomly selected larvae per age group. All age groups perform spontaneous slow and fast starts, often in combination with a change of swimming direction. We did not attempt to discriminate between spontaneous swimming bouts and behaviour elicited by external stimuli, such as other larvae; we therefore make no assumption about the neural control of these starts. Fast starts are often followed by an extended episode of cyclic fast swimming, which will be referred to as 'cyclic swimming' in the remainder of the text. For all age groups combined, we recorded 50 episodes of cyclic swimming (fish swims at a constant mean speed), 140 starts (fish accelerates from stand-still) and 10 coasts (fish decelerates). Of the 140 starts, 29 were so-called 'routine turns' (Budick and O'Malley, 2000), in which the fish adopted a C shape during the preparatory stroke to initiate a turn plus swimming bout. We made a selection from this extensive database to illustrate the flow patterns that characterise the different swimming modes.

Kinematic analysis

To map the swimming kinematics and the body wave, the midlines of the larval body were digitised using MatLab 7.0 (MathWorks, Inc., Natick, MA, USA) by manually indicating 20–25 points along the central axis of the larval silhouette. These raw midlines were interpolated and smoothed in space and time using a cubic spline fit (Woltring, 1986) to obtain 51 equidistant points [for a more detailed description of the interpolation, smoothing and smoothing-factor criteria, see Johnston et al. (Johnston et al., 1995)]. We then derived the mean path of motion by linear regression through the positions of the snout and the tail tip. From the interpolated midlines, we obtained several kinematic parameters following Müller and van Leeuwen (Müller and van Leeuwen, 2004): instantaneous and mean swimming speed (U_{inst} and U) and acceleration (a), tail-beat amplitude (A) and tail-beat frequency. From the lateral displacement wave, we also derived the wave of curvature. For more details, see Johnston et al. (Johnston et al., 1995) and Müller and van Leeuwen (Müller and van Leeuwen, 2004). The computer programs used to calculate the smoothed midlines, instantaneous swimming speed and acceleration, and body curvature were written in Fortran. All other kinematic

parameters were calculated from these data using command files written for MatLab 7.0 on a PC. Throughout the remainder of the text, all lengths are normalised by total body length (L); hence, tail-beat amplitude, swimming speed and acceleration are expressed as specific values, unless they are qualified as 'absolute' values.

To determine the precision of the digitising process, for the 2 d.p.f. group we digitised one sequence of each behaviour, five times. The standard errors of the mean tail-beat amplitude, mean swimming speed and curvature are always less than 0.05 (N=5). Position of maximum curvature along the body has a standard error of <0.01 (N=5) (Müller and van Leeuwen, 2004).

To map the motion of the centre of mass, we further determined the body shape of the zebrafish larvae (age 2–5 d.p.f.) from horizontal and lateral digital photographs (Olympus DP50 digital camera mounted on a Zeiss Stemi SV1 microscope). We measured the height and width of finfold, eye, yolksac and main body at 51 equidistant points along the body using MatLab 7.0. Based on these measurements, we modelled the total fish as comprising 50 elliptical segments of uniform mass density (ρ_{fish}=1000 kg m^{-3}). We determined the mass and centre of mass of each body segment, and then calculated the fish's centre of mass by numerical integration over all 50 segments, thereby taking into account body deformation [similar to the method of Jing et al. (Jing et al., 2004)]. Details of our method will be discussed in a forthcoming paper. Velocity and acceleration of the centre of mass were calculated by differentiation of the position data using quintic spline functions as described elsewhere (Woltring, 1986).

Particle image velocimetry analysis

We present data from six sequences, for which we did a complete kinematic plus digital particle image velocimetry (DPIV) analysis, and in which the fish swims either horizontally or vertically through the light sheet – sequences with an oblique swimming path were used only for qualitative comparison to test consistency of drawn conclusions. The six sequences were chosen to provide an overview of the flow events that take place during a complete episode of active swimming, from (1) the start of active swimming, over (2) swimming cyclically, to (3) the moment that the fish decelerates while it gradually ceases to undulate its body. We used a super-PIV routine (Hart, 1999), embedded in a custom MatLab 7.0 program to batch-process sequences of up to 300 frames. The size of the initial sub-image for the DPIV's correlation procedure was 32^2 pixels, and reduced to 16^2 for the second and final correlation. Overlap between sub-images is 50%. The fish was not masked, so the PIV correlation routine included pixels that comprise the fish, which normally reduces accuracy of the flow information adjacent to the fish. In our case, the fish is transparent and carries natural body-attached markers with it, unlike most adult fish, which form large black areas in PIV recordings due to their solid body and their cast shadow. By forming part of the 'flow' pattern, the larval body is processed by the PIV routine as part of the flow, leading to the non-slip condition being observed in our PIV analysis without any explicit implementation in the PIV algorithm. In the recorded sequences, the width of the fish's posterior body corresponded to 30 pixels at its widest point behind the yolk sac.

Results

A spontaneous routine swimming bout consists of three phases: the start, in which the fish accelerates from stand-still, a cyclic swimming phase, in which the fish swims at an approximately constant mean swimming speed, and a deceleration phase, in which the larva gradually comes to a stand-still.

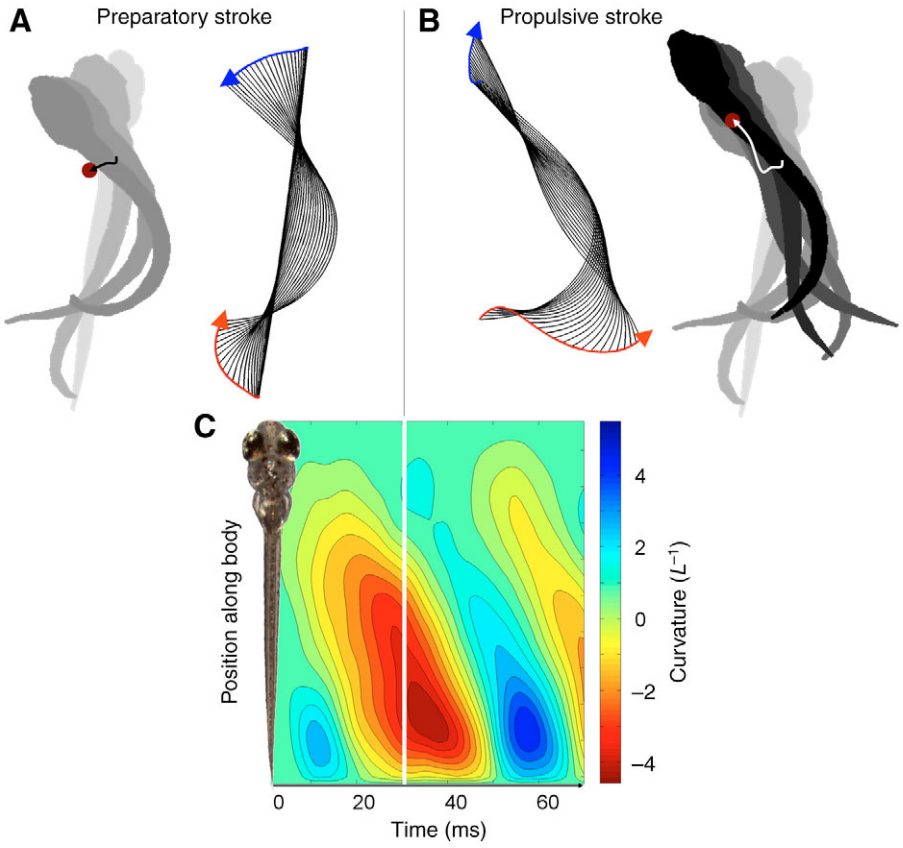

Fig. 1. C-start of a zebrafish larva (age 5 d.p.f., body length L=4.2 mm). Swimming kinematics. (A) During the preparatory stroke the body, represented by its midlines, adopts a C shape. Silhouettes (left, time step 10 ms) and midlines (right, time step 1 ms) of a fish larva. Black arrow, path of the centre of mass (dark red dot); blue arrow, path of head; red arrow, path of tail. (B) During the propulsive stroke the body straightens and the tail completes the first tail-beat cycle. Silhouettes (right, time step 10 ms) and path of the centre of mass are shown for preparatory plus propulsive stroke; midlines (left, time step 1 ms) are shown for the propulsive stroke only. White arrow, path of the centre of mass (dark red dot); blue arrow, path of head; red arrow, path of tail. (C) Curvature of the larval midline during a C-start. Body curvature increases steadily during the preparatory stroke; the propulsive stroke commences when the total concave curvature (red) reaches its maximum and the first body wave begins to form, visible as a convex curvature (blue) band that travels down the full length of the body. (Same sequence as Fig. 2.)

Initiating a swimming bout: flow generated by the first tail-beat cycle

When a zebrafish larva spontaneously initiates a swimming bout, its first tail-beat cycle often constitutes a so-called routine turn (Fig. 1A) (Budick and O'Malley, 2000). The body re-orients during the preparatory stroke, in which the body takes more than 15 ms to bend into less than a semi-circle (Fig. 1A,C) (Budick and O'Malley, 2000). The particular sequence shown in Figs 1 and 2 is of a 5-day old (L=4.4 mm) zebrafish larva during this first tail-beat cycle of the acceleration phase. During this particular preparatory stroke (t=0–23 ms), the body bending into a C shape causes a small lateral, but no forward, translation of the centre of mass (Fig. 1A, left panel). The larva reaches a peak angular speed of 21° ms^{-1} at time t=9 ms after the initiation of the swimming bout, and ultimately changes its heading by 44°. During the following propulsive stroke (t=23–67 ms), the body straightens (Fig. 1C) while the tail reverses to complete the tail-beat cycle, and the larva's centre of mass accelerates forward (Fig. 1B, right panel). The larva's forward speed peaks during the propulsive stroke at 0.030 m s^{-1} (7.0 L s^{-1}) at time t=39 ms.

The preparatory stroke generates a prominent jet flow towards the increasingly concave side of the body (Fig. 2; 10–20 ms, grey arrow). Furthermore, there form two weaker areas of fast flow at the head and the tail, which are induced by the lateral movement of head and tail (Fig. 2, white arrows). These local jets cause shear flows, and these shear flows cause four patches of elevated vorticity of alternating rotational sense to form along the bending body (Fig. 2; 10 ms). The vorticity patches travel through the water and

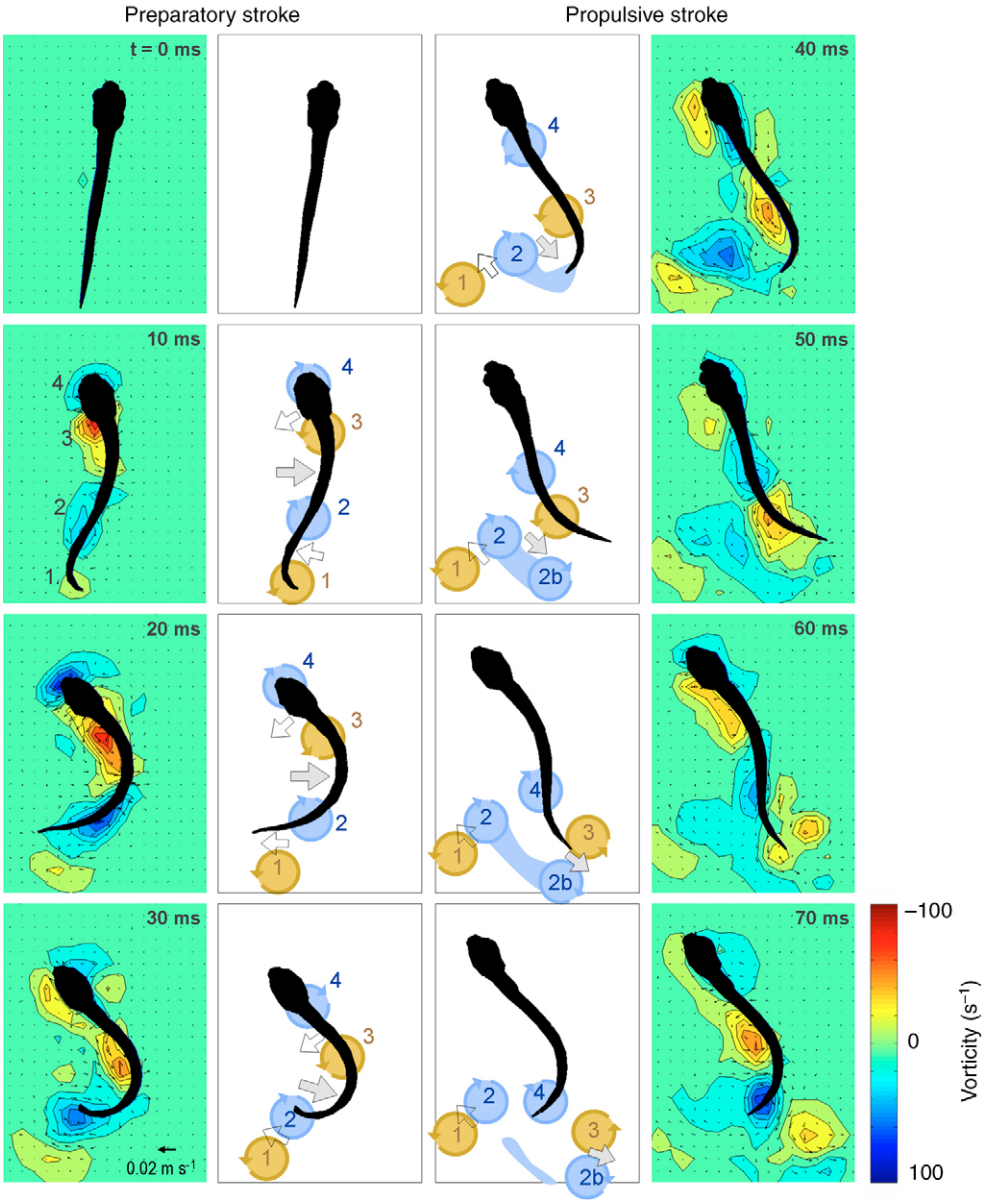

Fig. 2. Vorticity field (colour map) and flow velocities (black arrows) generated during the preparatory (left columns) and propulsive stroke (right columns) of a larval C-start (age 5 d.p.f., body length L=4.4 mm). The sketches beside the vorticity colour maps highlight the most relevant flow features. Over the entire C-start, the larva sheds two vortex pairs, one during the preparatory (vortices 1 and 2), and one during the propulsive stroke (vortices 2b and 3). By the time, the second pair is shed, the first pair has moved from its initial shedding position and has almost disappeared (70 ms, vorticity field). Grey arrow, jet into concave body bend; white arrows, other jets; blue circles: clockwise vortices; ochre circles, counter-clockwise vortices. (Same sequence as Fig. 1.)

down the body along with the wave of curvature, and are shed when they reach the tail.

During the preparatory stroke, the two most posterior patches of elevated vorticity (vortices 1 and 2) are shed in the wake. Vortex 1 is shed (Fig. 2; between 10 and 20 ms) as the tail region reaches maximum curvature (Fig. 1C; 12 ms) and begins to straighten half way through the preparatory stroke (Fig. 1C; 14 ms). Vortex 2 is shed at the end of the preparatory stroke, when the fish has adopted a C shape (Fig. 2; between 30 and 40 ms, blue vorticity patch 2). The shedding coincides with the tail decelerating. It occurs when lateral curvature, averaged along the body, peaks (Fig. 1C), and before the wave of curvature begins to travel more slowly down the posterior body. The two consecutively shed counter-rotating vortices 1 and 2 form a vortex pair in the horizontal cross section through the fish's wake, as indicated by the jet forming between the vortices (Fig. 2; 40 ms, vortices 1 and 2).

During the propulsive stroke of the first tail-beat cycle, a second vortex pair is shed, vortices 2b and 3. Vortex 2b forms as the tail transverses to complete the propulsive stroke. Behind the tail, a ribbon of clockwise (blue) vorticity forms in the wake. At the same time as the tail beats to the right, the body wave travels down the body, and with it a patch of counter-clockwise (ochre) vorticity. This patch is ultimately shed when it reaches the tail at the end of the propulsive stroke to form vortex 3. In the presence of vortex 3, the ribbon of clockwise vorticity forms into vortex 2b. Together, vortices 2b and 3 form a second vortex pair in the horizontal plane of the fish's wake (Fig. 2; 70 ms).

Over the course of the first tail-beat cycle, the two shed vortex pairs form to the left and right of the fish (Fig. 2; 70 ms). When looking at a horizontal cross-section of the vortex pairs shed by a larva turning by 40° at the start of a swimming bout, the vortex pair shed during the preparatory stroke has a larger cross-sectional area and higher vorticity than the vortex pair of the propulsive stroke at the respective moments of shedding (Fig. 2; 30 *vs* 60 ms). The vortices decline rapidly in strength after they are shed: the vorticity of the first vortex pair shed into the wake halves within 20 ms (Fig. 2; 40–70 ms). By the time the second vortex pair is shed 30 ms after the first pair (Fig. 2; 60–70 ms), the instantaneous maxima in the vortex pair's vorticity field have dropped to less than 30% of their original, maximum value. Both vortex pairs shed during the first tail-beat cycle have died off completely 150 ms after the initiation of the swimming bout and 90 ms after the second vortex pair had formed. The quick dying-off of the wake is a prominent effect of the significant viscous forces.

This qualitative flow pattern – two vortex pairs shed during the initial tail-beat cycle of the acceleration phase – was observed in 14 of the 29 recorded start-plus-turn sequences, which contained the complete wake. The remaining sequences only contained partial wakes because the larva was not swimming in a central portion of the camera's field of view. All sequences were recorded at age 3, 4 and 5 d.p.f. The vorticity contained in the vortices shed during the propulsive stroke of the first tail-beat cycle reaches maximum values of 50–100 s^{-1} at the moment of shedding (three vortex pairs from three start sequences, age 5 d.p.f.), and vorticity drops to less than 10 s^{-1} 50–90 ms after the vortices were shed.

During a swimming bout: flow generated while swimming cyclically

After a strong, spontaneous start, young zebrafish larvae continue to swim for at least three tail beats (Müller and van Leeuwen, 2004). During this so-called cyclic swimming, the fish larva undulates its body at an approximately constant tail-beat frequency and amplitude (Fig. 3A) and the larva's mean swimming speed (i.e. average over a complete tail beat) is constant. However, the larva's instantaneous swimming speed varies. At low mean swimming speeds (<20 $L\ s^{-1}$), instantaneous swimming speed can differ from mean swimming speed by as much as 50% (Müller and van Leeuwen, 2004). The larva shown in Figs 3, 4 (age 3 d.p.f., L=3.8 mm) swims at a mean speed of 18±2 $L\ s^{-1}$ (mean over four tail-beat cycles). Around this mean value, instantaneous swimming speed oscillates between 14 and 24 $L\ s^{-1}$. The larva undulates its body in a lateral wave that travels posteriorly with a mean wave speed V=53 $L\ s^{-1}$ that is three times the mean swimming speed U (ratio U/V=0.34), which is within the range of 0.15–0.55 typical for cyclic swimming (Müller and van Leeuwen, 2004). The body wave travels at an approximately constant speed along the posterior body, as visible in approximately straight waves of curvature (Müller and van Leeuwen, 2004) (Fig. 3B).

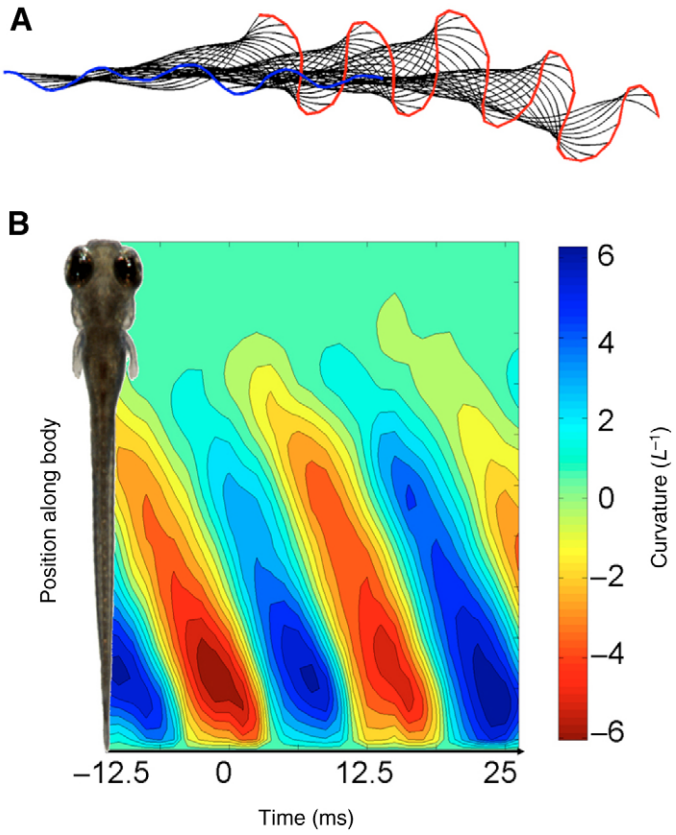

Fig. 3. Kinematics of a cyclically swimming zebrafish larva (age 3 d.p.f., body length L=3.8 mm). (A) The larva generates a body wave travelling down its body with a roughly constant tail-beat frequency and amplitude. Blue, path of the head, red, path of tail. (B) The body wave becomes prominent behind the stiffer anterior body and travels as a wave of curvature with a roughly constant speed along the posterior body. (Same sequence as Fig. 4.)

The flow pattern along the larval body differs markedly between the stiff anterior and the undulating posterior body (Fig. 4). The flow in the transverse and horizontal planes just in front of the snout behaves essentially like a source with water being pushed away from the snout laterally and forward (Fig. 4, Fig. 5A,C). The head and yolk sac are enveloped by a region of elevated vorticity [Fig. 4; right column shows only counter-clockwise vorticity (elongate ochre area), not the clockwise vorticity, of head and yolk-sac flow]. This vorticity along the anterior body is formed by the head's boundary layer, which separates at the eyes, but remains close to

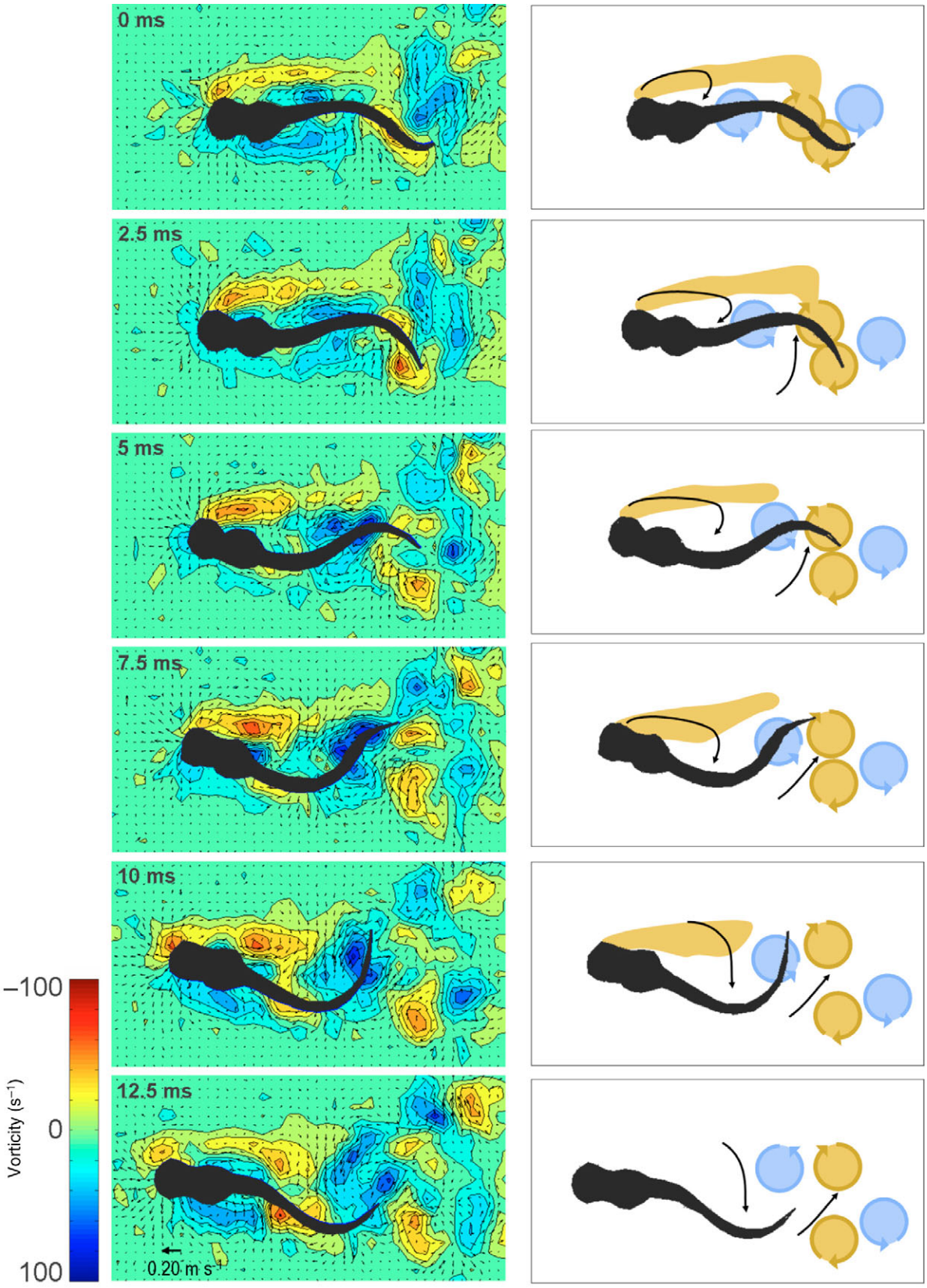

Fig. 4. Flow generated during a tail beat of a cyclically swimming zebrafish larva (age 3 d.p.f., body length *L*=3.8 mm). (Left) Vorticity field (colour map) and velocity vector field (black arrows) adjacent to a fish larva. (Right) Sketch of most relevant flow features. The drag wake of the anterior body (elongate ochre area in sketch) is prominent in the vorticity field throughout the tail-beat cycle. The two main propulsive features of the flow along the larva are (1) the jet into the concave bend of the body, which gradually reorients more caudally as it travels down the body (black arrows); (2) several smaller patches of vorticity along the posterior body, which are shed as two vortex pairs per tail-beat cycle (blue and ochre circles). (Same sequence as Fig. 3.)

the anterior body to form a drag wake. Vorticity in this separated boundary layer peaks at a distance of 0.1 *L* from the surface of the yolk sac. Boundary layer separation occurs continuously throughout the tail-beat cycle. But due to the yawing head motion, the location of the separation point oscillates, as does the location of the stagnation point on the snout. Yaw and oscillating swimming speed also cause oscillations in the flow pattern and the strength of the shed vorticity (Fig. 4).

At the transition from yolk sac to the much narrower posterior body, there forms a drag wake. The drag wake forms within the separated boundary layer of the head (Fig. 4, right column: elongate ochre patch along head and yolk sac), and is visible as flow velocity vectors immediately behind the yolk sac that are directed towards the yolk sac (Fig. 4, right column: leftmost black arrow, 0–5 ms). Further along the body, this drag wake interacts with the flow patterns generated by the undulating body. Hence, the boundary layer along the anterior body does not extend along the entire posterior body because the posterior body is undulating fast, generating an unsteady flow.

The flow pattern along the posterior body is dominated by the transverse undulations of the body and consequently varies strongly over one tail-beat cycle. The concave sides of the body wave generate strong flows towards the body similar to the concave side of the preparatory stroke of the initial tail-beat cycle (Fig. 4, right column: leftmost black arrow, 10–12.5 ms). In an undulating body, this results in a succession of localised jets (Fig. 4, right column: rightmost black arrow). The jets and areas of elevated flow velocity begin to form in the envelope of the drag wake along the anterior body: initially, the main flow still points towards the yolk sac. As the body wave travels down the body, the direction of the main flow in the jet turns increasingly sideways (Fig. 4, right column: leftmost black arrow). As a jet reaches the tail, its main flow is directed backward at an angle smaller than 90° with the larva's mean path of motion.

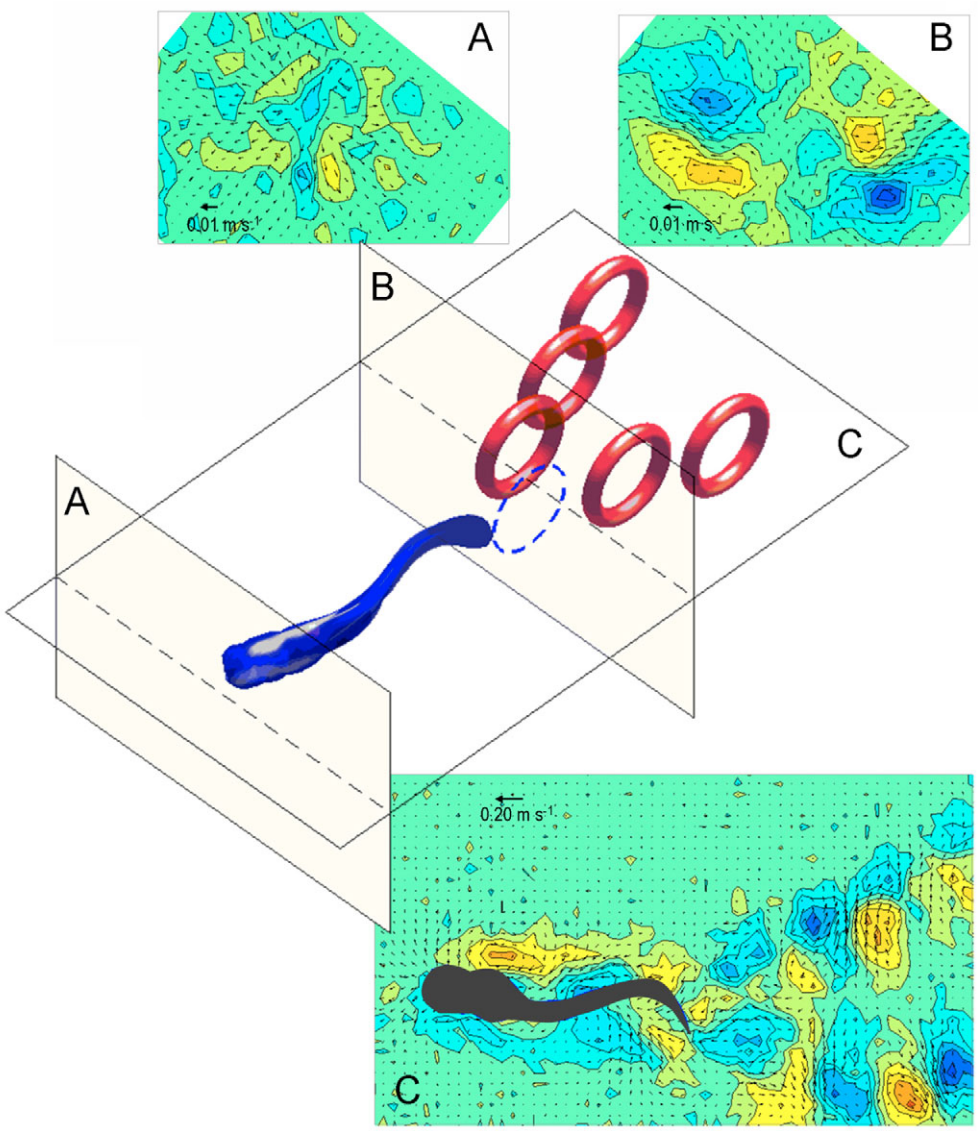

Fig. 5. Three-dimensional reconstruction of the wake behind the cyclically swimming zebrafish larva (age 3 d.p.f.) (overview panel; letters correspond to flow diagrams A–C). The vortex rings (red) shown in the overview panel take time to develop, so the ring immediately behind the tail has not yet fully formed (blue broken line), as is also evident in C. Transverse cross sections through the larval flow field (A) in front of and (B) behind the larva. (C) Horizontal cross-section through the larval wake. The stronger vortices are due to a slight turn (Fig. 3).

Each jet is framed by two areas of elevated vorticity of opposite rotational sense, one anterior and one posterior to the jet along the body (Fig. 4, right column; leftmost blue and ochre circle). These areas of vorticity travel along the body together with the body wave and are shed when they reach the tail. Shedding occurs when the tail reaches maximum lateral excursion [Fig. 4; 7.5–10 ms: shedding of vortex (top ochre circle in right panel)].

The total wake forms as a result of the interaction between the undulation-based wake shed off the tail (Fig. 4, right column; circular patches of vorticity) and the drag-based wake of the anterior body (Fig. 4, right column; elongate patch of vorticity). The tail-beat amplitude is wide enough for the tail to disrupt the ribbon of vorticity that developed from the separating boundary layer and consequently formed the drag wake of the anterior body (Fig. 4, right column; elongate area of head vorticity separates from circle of body vorticity between 2.5 and 5 ms). The tail sheds its patch of the undulation-based vorticity (Fig. 4, right column; bottom ochre circle: 2.5–5 ms). This shed vortex combines with a previously shed vortex of opposite rotational sense to form the first vortex pair of this tail-beat cycle (Fig. 4, right column; right blue circle: 5 ms). As the tail reverses direction and starts to beat to the right, a ribbon of clockwise vorticity remains attached to the tail. This vorticity is finally shed just prior to the tail reversing direction to beat from right to left (Fig. 4, right column; top ochre circle: 5–7.5 ms). As the tail reverses direction again, another vortex is shed (Fig. 4, right column; left blue circle: 10–12.5 ms). These two counter-rotating vortices form the second vortex pair shed during the tail-beat cycle shown. The jet between the two vortices forming a pair is oriented almost perpendicular to the mean path of motion (most clearly visible in Fig. 5C).

The larva sheds two vortex pairs per tail-beat cycle, one pair per lateral tail excursion. Each vortex pair forms off to the side from the mean path of motion and continues to move away from it under its own momentum. A horizontal section through the larva's three-dimensional wake exhibits two diverging rows of vortex pairs, one to either side of the mean path of motion (Fig. 5C). As the wake matures, the vortex pairs slow down and vorticity begins to fade, so that the wake reaches a width of 1–2 larval body lengths before it dies off completely. A transverse cross-section through the wake also reveals vortex pairs to the left and right of the mean path of motion (Fig. 5B). The total wake is roughly twice as wide as it is high. The wake dies off quickly: within 50 ms, vorticity and flow velocity levels are reduced below 10% of their maximum value.

This qualitative flow pattern – two vortex rings shed per tail-beat cycle – could be identified in 24 of 50 cyclic swimming sequences, of which 19 were horizontal and 5 vertical (1 lateral view and 4 transverse views) sections through the wake. In the remaining 26 recordings, changes in swimming speed and swimming direction obscured the regularity of the wake pattern, or the larva was swimming not in the centre of the camera view and light sheet, leaving only partial impressions of the wake or negative information (e.g. horizontal cross sections that were well above or

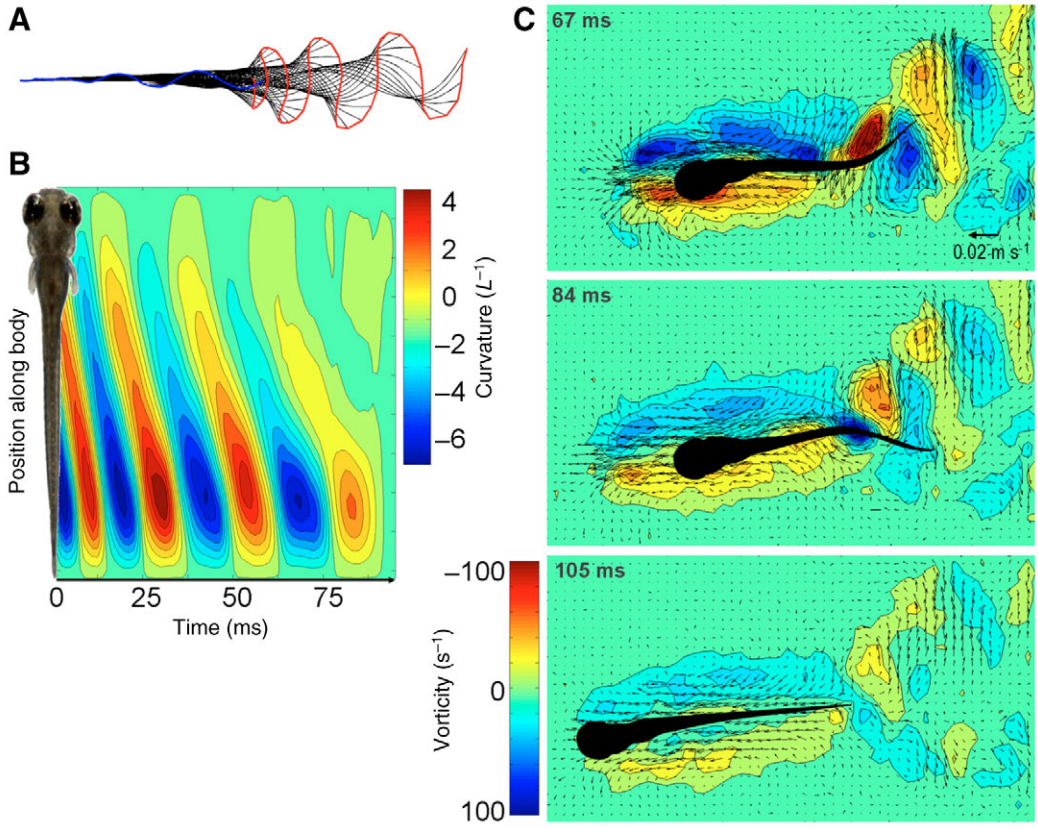

Fig. 6. Transition from cyclic swimming to coasting in a zebrafish larva (age 4 d.p.f., body length L=4.0 mm). (A) Amplitude envelope narrows, tail-beat frequency and stride length drop, as towards the end of an active swimming bout. (B) Peak curvature also decreases. Curvature of the body midline during the last four tail beats of a swimming bout. (C) The vorticity field (colour map) and velocity vector field (black arrows) adjacent to the larva show how the boundary layer increasingly engulfs the entire decelerating larva. Shown are the last two times that the tail reaches a lateral extreme (67 and 84 ms) and a coast flow field (105 ms). The times correspond to the time axis of B.

below the larva confirmed evidence from vertical cross sections about the limited height of the wake by not showing any significant flow). The cyclic swimming sequences were recorded at age 2, 3 and 4 d.p.f.

Deceleration phase

As the fish larva reaches the end of a swimming bout, it slows down by reducing its tail-beat amplitude and frequency. The sequence shown (Fig. 6) is of a 4 d.p.f. larva (L=4.0 mm) at the end of a cyclic swimming bout. The last tail beat consists of the tail returning to the mean path of motion (Fig. 6A). After the last tail beat, the terminal speed at end of a burst is 2.1 $L\,s^{-1}$. The larva reduces its tail-beat amplitude from 0.20 L to 0.15 L (Fig. 6A) and its tail-beat frequency from 44 Hz to 31 Hz over the last three tail-beat cycles, which can be seen in the body curvature wave: consecutive waves of curvature are slower, and curvature decreases (Fig. 6B).

The last tail beats generate vortex pairs (Fig. 6C) much like those observed during cyclic swimming (Fig. 5C). The most striking feature of the flow field around a decelerating larva is the large area of elevated vorticity surrounding the entire larva (Fig. 6C; 67 and 84 ms). As the tail-beat amplitude decreases during the last few tail beats, the tail no longer 'cuts' through the drag wake shed off the anterior body, and a continuous boundary layer begins to engulf the larva. Within the drag wake of the anterior body, the boundary layer along the posterior body grows much thicker than the larval body is wide, allowing us to visualise the distribution of vorticity within the growing boundary layer of the decelerating larva. This vorticity diffuses while the larva slows down.

The development of the thick boundary layer could be observed in all ten deceleration sequences, in the age groups 3, 4 and 5 d.p.f. In all sequences, the larvae reduced tail-beat amplitude and frequency. Average tail-beat frequency during cyclic swimming was 40±4 Hz (N=10), and it reduced to 30±3 Hz (N=10) over the last two tail-beat cycles.

Discussion

Relating flow and swimming behaviour in zebrafish larvae

Time-resolved recordings of the flow around a fish larva during a start and cyclic swimming show that fish larvae shed a vortex pair wake not dissimilar to that shed during a slow burst, during which zebrafish larvae employ a much lower tail-beat amplitude and tail-beat frequency (<20 Hz) (Müller et al., 2000; Müller and van Leeuwen, 2004).

Both types of start, fast starts initiating cyclic swimming and slow starts initiating a slow burst, generate a flow towards the bending body during the preparatory phase (Müller et al., 2000). Compared with the fast start, the slow burst has no strong preparatory stroke – the body does not form a C, but bends only in the posterior half (Müller and van Leeuwen, 2004). This weak bend does not generate a clearly visible vortex pair, equivalent to the first vortex pair during the preparatory stroke of a fast start (Müller et al., 2000). At the end of the first tail-beat cycle of the slow start, a vortex pair becomes visible, which is equivalent to the second vortex pair of the fast start.

Relating flow to kinematics

The main goal of our study was to relate flow patterns to swimming kinematics, in order to take a first step towards understanding undulatory propulsion in fish larvae. Wake cross-sections have often been used to estimate momentum (Müller et al., 1997; Tytell and Lauder, 2004; Drucker and Lauder, 1999; Drucker and Lauder, 2001). When an animal accelerates, the wake should contain net backward momentum (Tytell, 2004b). Decelerating animals should generate a wake with net forward momentum. When swimming cyclically, the fish generates on average equal thrust and drag forces over the swimming cycle, and in the wake forward and backward momentum should cancel. Cross-sections through the larval wake qualitatively agree with this expectation: when a larva performs a start, its centre of mass reaches maximum acceleration near the end of the propulsive stroke, and the wake shed during the propulsive stroke contains net backward flow. During cyclic swimming, the flow in the larval wake is directed mainly sideways. During coasting, no vortex wake forms behind the larva due to the low Reynolds number and the larva's elongate body. Yet, the flow adjacent to and behind the larva is mainly directed forward, consistent with the larva generating only drag. These agreements with expectations remain, however, qualitative because the three-dimensional structure and size of the wake is unknown.

Nevertheless, it is possible to correlate kinematic and flow events to explore possible propulsion mechanisms. During cyclic swimming, instantaneous swimming speed and hence larval kinetic energy oscillate (Müller and van Leeuwen, 2004). Peaks in swimming speed closely follow the moments at which the tail reaches maximum lateral excursion (Müller and van Leeuwen, 2004), and peaks in speed coincide with maximum acceleration of the tail and shedding of vorticity at the tail into the wake. Maximum acceleration of the fish's centre of mass peaks just prior to vortex shedding: thrust force appears to peak near the moment for vortex shedding at the tail.

Role of Reynolds number on flow and comparison to adult flow fields

Zebrafish larvae (age 2–5 d.p.f.) swim at Reynolds numbers between 10^1 and 10^3, whereas adult zebrafish swim at 10^3–10^4. Larvae approach the adult flow regime only briefly when they reach top escape speeds of 50–65 $L\,s^{-1}$. Most of the larval swimming behaviour, however, takes place at considerably lower Reynolds numbers, between 10^1 and 10^2, in the viscous and intermediate flow regime (Fuiman and Webb, 1988). Low Reynolds numbers are a likely explanation both for the comparatively simple, laminar wake and for the quick reduction of flow speeds in the wake. At Reynolds numbers well below 10^4, vortex rings are stable and not likely to break up (Van Dyke, 1982) while viscous diffusion removes all traces of even the most vigorous 'escape response' wakes within less than 0.5 s of the wake being shed. Low Reynolds numbers cause yet another important difference between larval and adult fish: larvae have a much thicker boundary layer relative to their body size than adults (Vogel, 1994). When swimming cyclically or coasting, fish larvae are enveloped by a boundary layer whose thickness is comparable to their body width. Hence, when recording total larval flow fields using PIV, the larval boundary layer is clearly visible, including the velocity and vorticity gradients within the boundary layer. In adult fish, the boundary layer is much thinner relative to the fish's body size and therefore not readily visible in overview flow fields of the fish (Anderson et al., 2001).

Reynolds number effects are less prominent during unsteady swimming behaviours, such as starts from stand-still: larval and adult danios generate similar vortex shedding patterns during routine turns – two vortex pairs in the horizontal plane through the wake [giant danio *Danio malabarius* (Wolfgang et al., 1999); zebrafish *Danio rerio* (Müller et al., 2000)]. No comparison is yet possible for cyclic swimming, because no flow fields have been

reported for adult zebrafish swimming steadily, partly because adult zebrafish rely more on burst-and-coast rather than steady swimming. However, a similar wake to that of larval zebrafish – two separate vortex rings per tail beat – can also be observed behind juvenile and adult eel (Müller et al., 2001; Tytell and Lauder, 2004). These eels swim at much higher Reynolds numbers of around 10^4 and therefore have a relatively thin boundary layer. Despite the differences in Reynolds number, and hence in relative boundary layer thickness and in vortex stability, both eel and zebrafish larvae shed a similarly simple wake; the wake's horizontal cross-section consists of vortex pairs shed to the left and right of the mean path of motion. This similarity might be due to a similar body shape and body wave kinematics. Both eel and zebrafish larvae have a long slender body with a finfold. This fin shape reduces the number of trailing edges to the tail only and hence might result in a simple wake shape. In that they differ from sunfish, for example, with their distinct unpaired fins, all of which shed their own wakes off their trailing edges (Tytell, 2006), and these individual wakes interact to form a complex total wake. In eel and zebrafish larvae, the simple trailing edge geometry of both fish and the low Reynolds numbers of zebrafish larvae might contribute to the less complex wake structure.

Eel and zebrafish larvae not only share an anguilliform locomotory morphology, but also the corresponding swimming mode. This anguilliform swimming mode is associated with a higher Strouhal numbers (adult eel, 0.3–0.4; larval zebrafish, 0.35–2.0), compared with so-called carangiform swimmers (0.08–0.35) (Triantafyllou et al., 1991; Taylor et al., 2003) such as mullet (Müller et al., 2001) and mackerel (Nauen and Lauder, 2002). Strouhal number can be calculated as the ratio of oscillation frequency and amplitude of the trailing edge to forward speed. With the vortices shed off the oscillating trailing edges at maximum lateral excursion, the ratio of oscillation frequency to stride length has an effect on the spatial distribution of the shed vortices and hence on wake shape (Triantafyllou et al., 2000). When a wake is shed off a trailing edge that moves with the tail-beat frequency and stride length of an anguilliform swimmer at high Strouhal numbers, then the shed vortices might form a vortex ring wake (as shown in Fig. 5), even in carangiform fish [adult great danio, Strouhal number 0.45 (Wolfgang et al., 1999)], whereas when the trailing edge moves like that of a carangiform swimmer at low Strouhal numbers, then the shed vortices might form a vortex chain wake, in which the vortex rings are linked to form a continuous chain (Blickhan et al., 1992).

To sum up, the larval wake differs from the adult wake in several ways for at least two possible reasons. First, there are differences due to Reynolds number: the wake might be relatively simple because the flow is laminar and vortices are unlikely to break up, and the wake dies off quickly. Second, differences might arise from morphological and kinematic differences: the larval wake contains relatively few patches of vorticity because fish larvae with their continuous finfold shed vorticity off relatively few trailing edges compared with adult fish that have distinct unpaired fins; the vortices in the larval wake assemble into a vortex pair wake because the larvae swim at a relatively high Strouhal number.

We would like to thank de Haar Vissen for breeding and maintaining the zebrafish. The manuscript was much improved by comments from David Lentink and from the anonymous referees. U.K.M. was funded by NWO grant number 814.02.006.

References

Anderson, E. J., McGillis, W. R. and Grosenbaugh, M. A. (2001). The boundary layer of swimming fish. *J. Exp. Biol.* **204**, 81-102.
Blickhan, R., Krick, C., Zehren, D. and Nachtigall, W. (1992). Generation of a vortex chain in the wake of a subundulatory swimmer. *Naturwissenschaften* **79**, 220-221.
Brackenbury, J. (2001). The vortex wake of the free-swimming larva and pupa of *Culex pipiens* (Diptera). *J. Exp. Biol.* **204**, 1855-1867.
Brackenbury, J. (2002). Kinematics and hydrodynamics of an invertebrate undulatory swimmer: the damsel-fly larva. *J. Exp. Biol.* **205**, 627-639.
Brackenbury, J. (2003). Swimming kinematics and wake elements in a worm-like insect: the larva of the midge *Chironomus plumosus* (Diptera). *J. Zool.* **260**, 195-201.
Brackenbury, J. (2004). Kinematics and hydrodynamics of swimming in the mayfly larva. *J. Exp. Biol.* **207**, 913-922.
Budick, S. A. and O'Malley, D. M. (2000). Locomotor repertoire of the larval zebrafish: swimming, turning and prey capture. *J. Exp. Biol.* **203**, 2565-2579.
Drucker, E. G. and Lauder, G. V. (1999). Locomotor forces on a swimming fish: three-dimensional vortex wake dynamics quantified using digital particle image velocimetry. *J. Exp. Biol.* **202**, 2393-2412.
Drucker, E. G. and Lauder, G. V. (2001). Locomotor function of the dorsal fin in teleost fishes: experimental analysis of the wake forces in sunfish. *J. Exp. Biol.* **204**, 2943-2958.
Drucker, E. G. and Lauder, G. V. (2005). Locomotor function of the dorsal fin in rainbow trout: kinematic patterns and hydrodynamic forces. *J. Exp. Biol.* **208**, 4479-4494.
Fuiman, L. A. (2002). Special considerations of fish eggs and larvae. In *Fishery Science: The Unique Contributions of Early Life Stages* (ed. L. A. Fuiman and R. G. Werner), pp. 1-32. Oxford: Blackwell.
Fuiman, L. A. and Batty, R. S. (1997). What a drag it is getting cold: partitioning the physical and physiological effects of temperature on fish swimming. *J. Exp. Biol.* **200**, 1745-1755.
Fuiman, L. A. and Webb, P. W. (1988). Ontogeny of routine swimming activity and performance in zebra danios (Teleostei: Cyprinidae). *Anim. Behav.* **36**, 250-261.
Gopalkrishnan, R., Triantafyllou, M. S., Triantafyllou, G. S. and Barrett, D. S. (1994). Active vorticity control in a shear flow using a flapping foil. *J. Fluid Mech.* **271**, 1-21.
Hart, D. P. (1999). Super-resolution PIV by recursive local-correlation. *J. Visualization* **10**, 1-10.
Jing, J., Yin, X. and Lu, X. (2004). Hydrodynamic analysis of C-start in crucian carp. *J. Bionics Eng.* **1**, 102-107.
Johnston, I. A., van Leeuwen, J. L., Davies, M. L. F. and Beddow, T. (1995). How fish power predatory fast-starts. *J. Exp. Biol.* **198**, 1851-1861.
Liao, J. C., Beal, D. N., Lauder, G. V. and Triantafyllou, M. S. (2003). The Kármán gait: novel body kinematics of rainbow trout swimming in a vortex street. *J. Exp. Biol.* **206**, 1059-1073.
McHenry, M. J. and Lauder, G. V. (2005). The mechanical scaling of coasting in zebrafish (*Danio rerio*). *J. Exp. Biol.* **208**, 2289-2301.
McHenry, M. J., Azizi, E. and Strother, J. A. (2003). The hydrodynamics of locomotion at intermediate Reynolds numbers: undulatory swimming in ascidian larvae (*Botrylloides* sp.). *J. Exp. Biol.* **206**, 327-343.
Müller, U. K. and van Leeuwen, J. L. (2004). Swimming of larval zebrafish: ontogeny of body waves and implications for locomotory development. *J. Exp. Biol.* **207**, 853-868.
Müller, U. K., van den Heuvel, B. L. E., Stamhuis, E. J. and Videler, J. J. (1997). Fish foot prints: morphology and energetics of the wake behind a continuously swimming mullet (*Chelon labrosus*). *J. Exp. Biol.* **200**, 2893-2906.
Müller, U. K., Stamhuis, E. J. and Videler, J. J. (2000). Hydrodynamics of unsteady fish swimming and the effects of body size: comparing fish larvae and adults. *J. Exp. Biol.* **203**, 193-206.
Müller, U. K., Smit, J., Stamhuis, E. J. and Videler, J. J. (2001). How the body contributes to the wake in undulatory fish swimming: flow fields of a swimming eel (*Anguilla anguilla*). *J. Exp. Biol.* **204**, 2751-2762.
Müller, U. K., Stamhuis, E. J. and Videler, J. J. (2002). Riding the waves: the role of the body wave in undulatory fish swimming. *Integr. Comp. Biol.* **42**, 981-987.
Nauen, J. C. and Lauder, G. V. (2002). Hydrodynamics of caudal fin locomotion by chub mackerel, *Scomber japonicus* (Scombridae). *J. Exp. Biol.* **205**, 1709-1724.
Taylor, G. I. (1952). The action of waving cylindrical tails in propelling microscopic organisms. *Proc. R. Soc. Lond. A Math. Phys. Sci.* **211**, 225-239.
Taylor, G. K., Nudds, R. L. and Thomas, A. L. R. (2003). Flying and swimming animals cruise at a Strouhal number tuned for high power efficiency. *Nature* **425**, 707-711.
Triantafyllou, M. S., Triantafyllou, G. S. and Gopalkrishnan, R. (1991). Wake mechanics for thrust generation in oscillating foils. *Phys. Fluids A* **3**, 2835-2837.
Triantafyllou, M. S., Triantafyllou, G. S. and Yue, D. P. K. (2000). Hydrodynamics of fishlike swimming. *Annu. Rev. Fluid Mech.* **32**, 33-53.
Tytell, E. D. (2004a). The hydrodynamics of eel swimming. II. Effect of swimming speed. *J. Exp. Biol.* **207**, 3265-3279.
Tytell, E. D. (2004b). Kinematics and hydrodynamics of linear acceleration in eels, *Anguilla rostrata*. *Proc. R. Soc. Lond. B Biol. Sci.* **271**, 2535-2540.
Tytell, E. D. (2006). Median fin function in bluegill sunfish *Lepomis macrochirus*: streamwise vortex structure during steady swimming. *J. Exp. Biol.* **209**, 1516-1534.
Tytell, E. D. and Lauder, G. V. (2004). The hydrodynamics of eel swimming. I. Wake structure. *J. Exp. Biol.* **207**, 1825-1841.
Van Dyke, M. (1982). *An Album of Fluid Motion*. Stanford: The Parabolic Press.
Videler, J. J. (1993). *Fish Swimming*. London: Chapman & Hall.
Vogel, S. (1994). *Life in Moving Fluids*. Princeton: Princeton University Press.
Webb, P. W. and Weihs, D. (1986). Functional locomotor morphology of early-life-history stages of fishes. *Trans. Am. Soc.* **115**, 115-127.
Wolfgang, M. J., Anderson, J. M., Grosenbaugh, M. A., Yue, D. K. P. and Triantafyllou, M. S. (1999). Near-body flow dynamics of swimming fish. *J. Exp. Biol.* **202**, 2302-2327.
Woltring, H. J. (1986). A Fortran package for generalised, cross-validatory spline smoothing and differentiation. *Arch. Eng. Softw.* **8**, 104-113.